Int J Adv Manuf Technol (2016) 86:1841–1851
DOI 10.1007/s00170-015-8267-8

ORIGINAL ARTICLE

Methods and results regarding sinusoid modulated pulse gas metal arc welding

Leilei Wang[1] · **Gongchun Heng**[1] · **Hui Chen**[1] · **Jiaxiang Xue**[1] · **Fanglue Lin**[1] · **Wenjin Huang**[1]

Received: 16 July 2015 / Accepted: 17 December 2015 / Published online: 12 January 2016

Abstract In this investigation, a sinusoid modulated pulse gas metal arc welding (SP-GMAW) method based on a current waveform control method and on the welding mechanism of pulsed gas metal arc welding (P-GMAW) was proposed. This method achieved smooth control over the welding current. The process formulas were simplified. Then, the control parameters were discussed and optimized. Finally, three comparison experiments were conducted. The results indicated that the SP-GMAW method, as an improved double-pulsed gas metal arc welding (DP-GMAW) method, had the following features: The SP-GMAW minimized porosity rate and generated palpable weld ripples in contrast with the P-GMAW. The SP-GMAW produced the finest fusion zone grain, highest fusion zone microhardness, and highest tensile strength among three welding methods. The feasibility and superiority of the method for welding aluminum sheet were verified.

Keywords Sinusoid modulated · Aluminum sheet · Welding process stability · Microstructure · Mechanical property

1 Introduction

Strong, high-quality welds of lightweight engineering alloys are playing an increasingly important role in modern manufacturing [1, 2]. Therefore, many countries have increased their focus on producing defect-free, structurally sound, and reliable joints of lightweight dissimilar alloys. Lightweight aluminum alloys are increasingly replacing steels. Consequently, advanced welding of aluminum alloys is recognized as an important requirement for producing various metallic components in the manufacturing sector [3]. High-strength aluminum alloy sheets with thicknesses of 3 mm or less have been increasingly used, particularly in the automotive industry [4–8]. The use of these sheets has motivated research on sheet welding technologies. Aluminum alloys have a low melting point and high thermal conductivity, and these alloys are easily distorted or burned through during welding processes [9–11]. Furthermore, to implement the welding of a compact oxide film on the surface of aluminum alloys, the cathode atomization effect resulting from an intense heat source is required. Therefore, the heat input into the base metal must be strictly controlled [12]. The welding power supply should not only ensure welding stability and form aesthetic welding seam, but it should also reduce the heat input and decrease deformation during the welding process [13, 14]. Higher requirements for energy control during welding have been proposed. However, an improper current input will readily cause an unstable welding process and produce weld defects, particularly when welding aluminum alloy sheets with thicknesses of 3 mm or less.

Researchers worldwide have continuously made improvements on welding equipment and welding processes. The emergence of pulsed gas metal arc welding (P-GMAW) is a representative example, and both P-GMAW and double-pulsed gas metal arc welding (DP-GMAW) can meet the demands for welding aluminum alloys [15, 16]. For aluminum alloys, the P-GMAW will easily produce hydrogen cracking in welds, and there are still problems in terms of parameter

✉ Jiaxiang Xue
mejiaxue@scut.edu.cn

[1] School of Mechanical and Automotive Engineering, South China University of Technology, Guangzhou, China

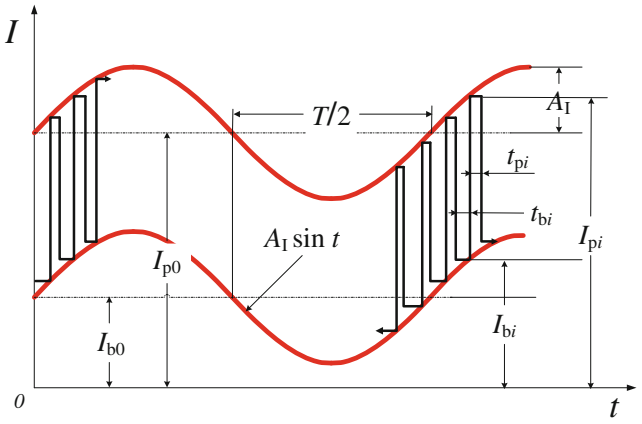

Fig. 1 Diagrammatic sketch of the SP-GMAW with parameters

matching, welding stability, and other issues [17, 18]. Researchers have begun to focus on the DP-GMAW, which reduces the cracking susceptibility, minimizes porosity rate, and results in aesthetic welding beads [19, 20]. Liu et al. [19] have surveyed arc length variation curve of the DP-GMAW. The results show that the arc length reaches maximum and wire extension reaches minimum from thermal peak phase to thermal base phase in constant wire-feed mode; meanwhile, mean current drops sharply in conventional rectangular thermal modulation. As a result, arc quenching rate increases obviously at this time during the actual welding process, particularly when the base metal is cold.

Vilarinho et al. [21] have proposed a trapezoidal thermal modulation based on conventional rectangular thermal modulation with the mean current gradually decreasing from the thermal peak phase to the thermal base phase. Wang et al. [22] and Liu et al. [23] have adopted this trapezoidal thermal modulation for welding aluminum alloys; high-quality joints are produced. Inspired by the evolution process from conventional rectangular thermal modulation to trapezoidal thermal modulation, a smooth thermal modulation concept is innovated. A sine function can derivate in an arbitrary order, naturally leading to the proposal of a sinusoid modulated pulse gas metal arc welding (SP-GMAW). The welding process of the SP-GMAW is more stable and reliable than that of the DP-GMAW [24]. Feasibility of welding 1-mm-thick aluminum sheet by the SP-GMAW also has been verified [25]. The SP-GMAW originates from the DP-GMAW; as an improved DP-GMAW, the SP-GMAW can be upgraded from the DP-GMAW by welding power supply

Table 1 Chemical compositions of AA6061 and ER4043 (wt.%)

Material	Si	Fe	Cu	Mn	Mg	Zn	Ti	Al
AA6061	0.561	0.289	0.31	0.052	0.986	0.024	0.018	Bal.
ER4043	5.6	0.8	0.30	0.05	0.05	0.10	0.20	Bal.

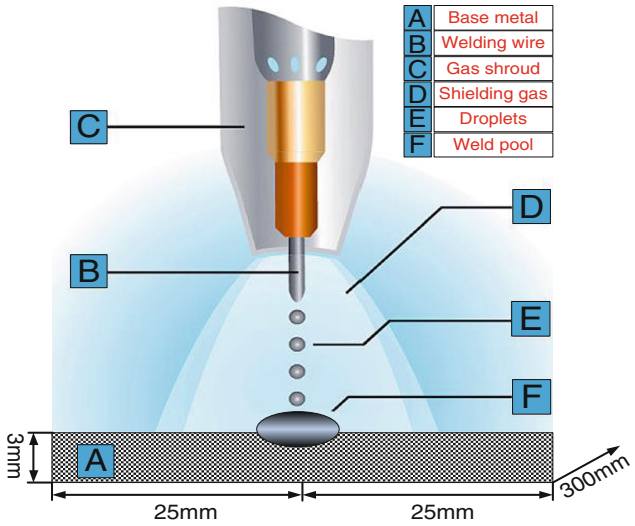

Fig. 2 Diagrammatic sketch of joint design with dimension

manufacturers without additional equipment, and the higher welding process stability for aluminum alloy is achieved.

However, literatures reveal that not much relevant researches have been done in the area of aluminum alloy weld quality produced by the SP-GMAW. The present investigation aims to introduce methodology and analyze the results of the SP-GMAW.

2 Mathematical model and control parameters of the SP-GMAW

The current waveform of the SP-GMAW is illustrated in Fig. 1.

The peak current and the peak time are as follows:

$$I_{pi} = I_{p0} + A_I sin(2\pi t_i/T)(i = 1, 2, \ldots, N) \quad (1)$$

Fig. 3 Experimental setup

Table 2 Welding conditions and process parameters

Welding method	P-GMAW	DP-GMAW	SP-GMAW
Mean current (A)	95	95	95
Mean voltage (V)	20	20	20
Gas flow rate (L/min)	15	15	15
Wire feed rate (m/min)	3.3	3.3	3.3
Electrode extension (mm)	15	15	15
Frequency (Hz)	81	3	3
Welding speed (cm/min)	45	45	45

$$t_{pi} = t_{p0} + A_{tp} sin(2\pi t_i/T)(i = 1, 2, \ldots, N) \quad (2)$$

Where I_{pi} is the peak current, I_{p0} is the initial peak current, t_{pi} is the peak time, t_{p0} is the initial peak time, A_I is the amplitude of the peak current, A_{tp} is the amplitude of the peak time, T is the cycle, and N is the number of current pulses in a sinusoidal cycle.

Similarly, the base current and base time are defined as follows:

$$I_{bi} = I_{b0} + A_I \sin(2\pi t_i/T)(i = 1, 2, \ldots, N) \quad (3)$$

$$t_{bi} = t_{b0} - A_{tb} \sin(2\pi t_i/T)(i = 1, 2, \ldots, N) \quad (4)$$

Where I_{bi} is the base current, I_{b0} is the initial base current, t_{bi} is the base time, t_{b0} is the initial base time, A_I is the amplitude of the base current, A_{tb} is the amplitude of the base time, and T is the cycle.

For the SP-GMAW process, regardless of how the current amplitude and pulse frequency are modulated, the overall goal is to control the input energy. Typically, it is not necessary to simultaneously modulate the current amplitude and pulse frequency.

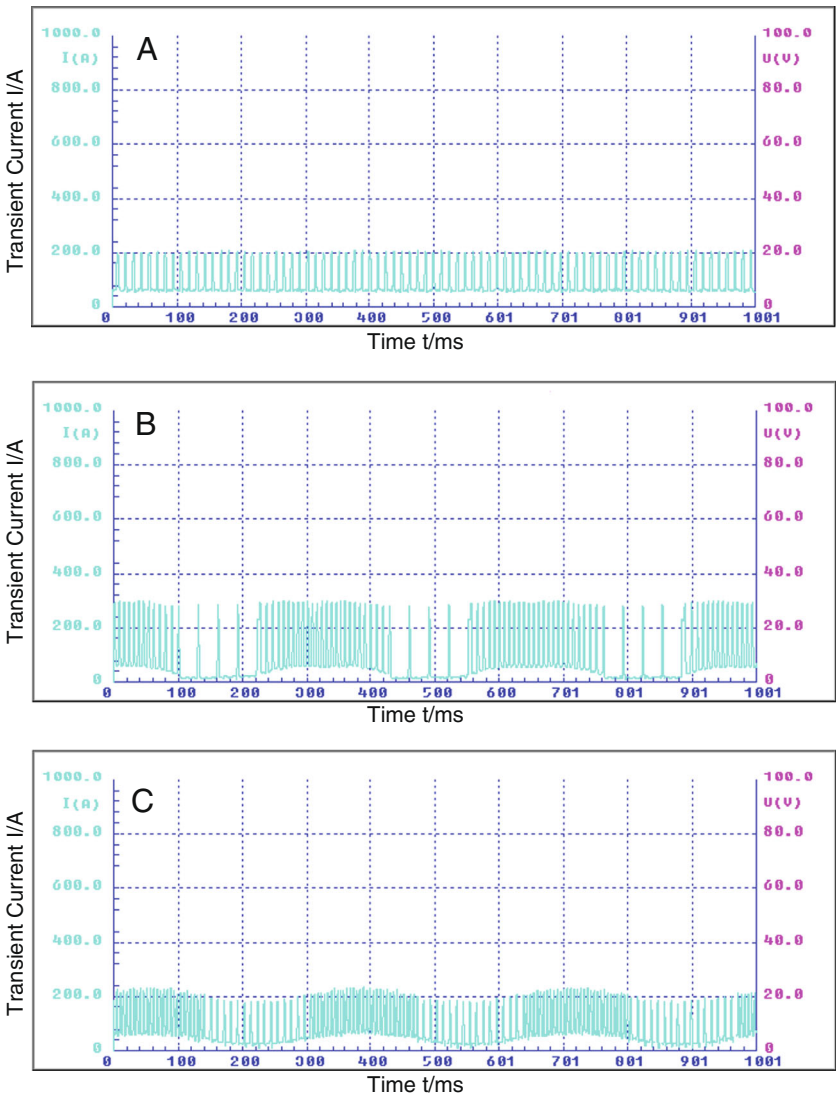

Fig. 4 Transient current waveforms: **a** P-GMAW. **b** DP-GMAW. **c** SP-GMAW

3 Simplifying the SP-GMAW

Because there are many complicated parameters in the SP-GMAW process, when the modulated current and its lasting time are at a peak or base at the same time, the energy input in a sinusoidal cycle will significantly change, which will affect the smooth energy transformation. Therefore, the SP-GMAW process can be controlled by modulating only one parameter, which simplifies setting the parameters.

For example, to simplify the control process, while keeping the peak time and base time unchanged, we assign $t_{pi}=t_0$, $t_{bi}=kt_0$, and $A_{tp}=A_{tb}=0$; then, the mathematical formula is simplified:

$$I_{pi} = I_{p0} + A_I \sin(2\pi t_i/T)(i = 1, 2, \ldots, N) \quad (5)$$

$$t_{pi} = t_{p0} = t_0(i = 1, 2, \ldots, N) \quad (6)$$

$$I_{bi} = I_{b0} + A_I \sin(2\pi t_i/T)(i = 1, 2, \ldots, N) \quad (7)$$

$$t_{bi} = t_{b0} = kt_0(i = 1, 2, \ldots, N) \quad (8)$$

In addition, both the peak time t_{pi} and the base time t_{bi} are determined. In one sinusoidal cycle T, both the thermal peak phase and thermal base phase time are kept equal to $T/2$. Assuming that the total number of pulses is N, the number of pulses in a sinusoidal thermal peak phase is $2*N/3$, and the number of pulses in a sinusoidal thermal base phase is $N/3$. If k_1 in a sinusoidal thermal peak phase is 2, then k_2 in a sinusoidal thermal base phase is calculated to be 5.

To ensure that the SP-GMAW process is smooth, the smallest peak current $I_{p\ \min}$ was selected based on previous welding experiments. Then, the initial peak current I_{p0} was confirmed. Simultaneously, to maintain the pilot arc current, the smallest base current $I_{b\ \min}$ was selected based

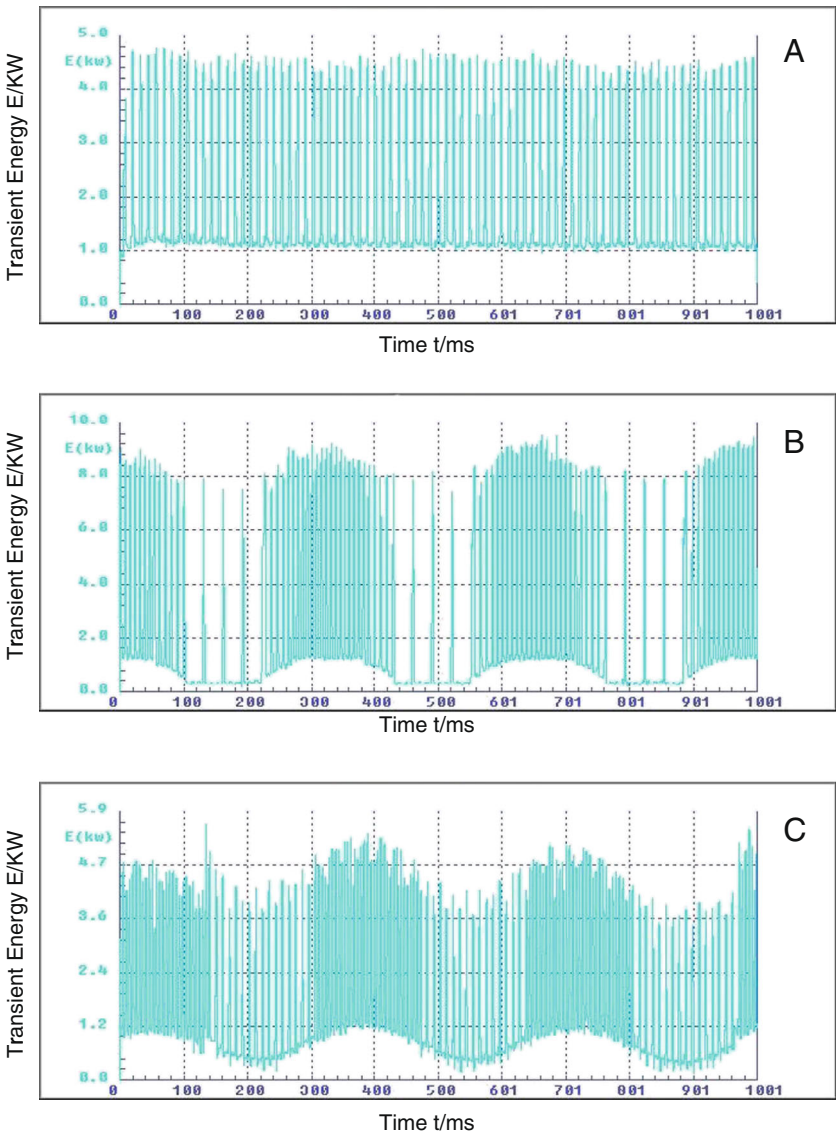

Fig. 5 Transient energy waveforms: **a** P-GMAW. **b** DP-GMAW. **c** SP-GMAW

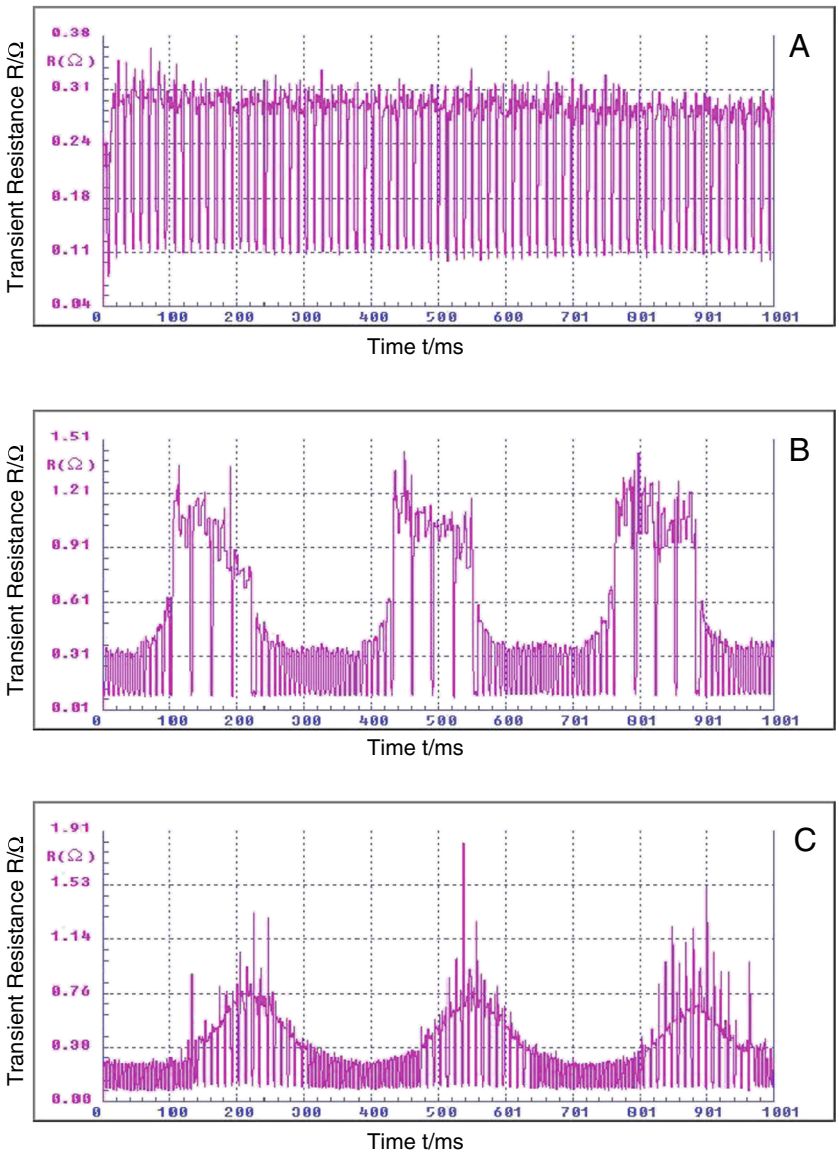

Fig. 6 Transient resistance waveforms: **a** P-GMAW. **b** DP-GMAW. **c** SP-GMAW

on previous welding experiments. Then, the initial base current I_{b0} was confirmed.

$$I_{p0} = I_{p\ \min} + A_I \tag{9}$$

$$I_{b0} = I_{b\ \min} + A_I \tag{10}$$

Thus far, the following parameters of the SP-GMAW process have been simplified: t_0, A_I, and N. In addition, the cycle is:

$$\begin{aligned} T &= \frac{2N}{3}(k_1 t_0 + t_0) + \frac{N}{3}(k_2 t_0 + t_0) \\ &= \frac{2N}{3}(2t_0 + t_0) + \frac{N}{3}(5t_0 + t_0) \\ &= 4Nt_0 \end{aligned} \tag{11}$$

A mathematical model of the SP-GMAW process was established by analyzing and simplifying the parameters of

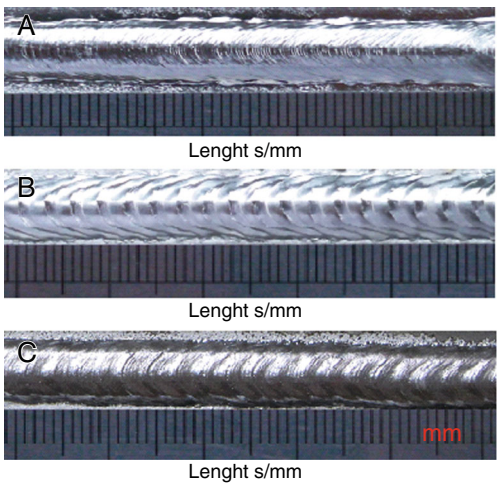

Fig. 7 Weld appearances: **a** P-GMAW. **b** DP-GMAW. **c** SP-GMAW

Fig. 8 Cross section of welds: **a** P-GMAW. **b** DP-GMAW. **c** SP-GMAW

the SP-GMAW process. Modulation of the current amplitude could be realized by controlling the following parameters: peak time t_0, current amplitude A_I, and the number of pulses in a modulated cycle N.

Different parameters will generate different welding seams. The fundamental reason for this phenomenon is that the welding energies are diverse. The average welding current is commonly considered to be a measurement of the actual welding energy. The most widely used equation for computing the average welding current is as follows:

$$\begin{aligned}\overline{I} &= \frac{\sum_{i=1}^{N}\left(t_{pi}I_{pi}+t_{bi}I_{bi}\right)}{T} \\ &= \frac{\sum_{i=1}^{N}t_{pi}I_{pi}+\sum_{i=1}^{N}t_{bi}I_{bi}}{T} \quad (i=1,2,\ldots,N)\end{aligned} \tag{12}$$

Substituting Eqs. (5) to (11) into Eq. (12), after arrangement, the average welding current can be expressed as:

$$\begin{aligned}\overline{I} &= \frac{\sum_{i=1}^{N}t_{pi}I_{pi}+\sum_{i=1}^{N}t_{bi}I_{bi}}{T} \\ &= \frac{\begin{array}{l}\sum_{i=1}^{N}t_0\left[I_{p0}+A_I\sin(2\pi t_i/T)\right] \\ +\sum_{i=1}^{2N/3}2t_0[I_{b0}+A_I\sin(2\pi t_i/T)] \\ +\sum_{i=(2N/3)+1}^{N}5t_0[I_{b0}+A_I\sin(2\pi t_i/T)]\end{array}}{4Nt_0} \\ &= \frac{\begin{array}{l}\sum_{i=1}^{N}\left[I_{p0}+A_I\sin(2\pi t_i/4Nt_0)\right] \\ +\sum_{i=1}^{2N/3}2[I_{b0}+A_I\sin(2\pi t_i/4Nt_0)] \\ +\sum_{i=(2N/3)+1}^{N}5[I_{b0}+A_I\sin(2\pi t_i/4Nt_0)]\end{array}}{4N} \\ &\left(i=1,2,\ldots,N\right)\end{aligned} \tag{13}$$

In the above equation, $I_{p0}=I_{p\ \min}+A_I$ and $I_{b0}=I_{b\ \min}+A_I$. After t_0 was selected, the corresponding value of $I_{p\ \min}$ was chosen from the one droplet per pulse critical curve, and the corresponding value of $I_{b\ \min}$ was chosen from the pilot arc critical curve.

Equation (13) clearly indicates that the average current is determined by t_0, N, $I_{p\ \min}$, $I_{b\ \min}$, and A_I and that the cycle time is determined by t_0 and N. However, this conclusion is obtained based on the SP-GMAW model, and verification tests are required to confirm it.

4 Experimental procedures

To demonstrate the feasibility of the SP-GMAW method for aluminum alloy sheets, three comparison experiments were conducted.

4.1 Materials

The sheets of a commercial AA6061 aluminum alloy with a dimension of 200 × 50 × 3 (mm) were used in this study, and an ER4043 filler wire with a diameter of 1.2 mm was adopted to deposit the seam. The chemical compositions of the base metal and filler wire are presented in Table 1. Joint design with dimension is illustrated in Fig. 2.

4.2 Welding equipment

A self-developed digital multifunctional welding power supply was selected as the welding power supply in this experiment. Measurements of the current and voltage were performed using a self-developed arc dynamic wavelet analyzer. The arc dynamic wavelet analyzer could calculate the transient energy, transient resistance and arc signal probability

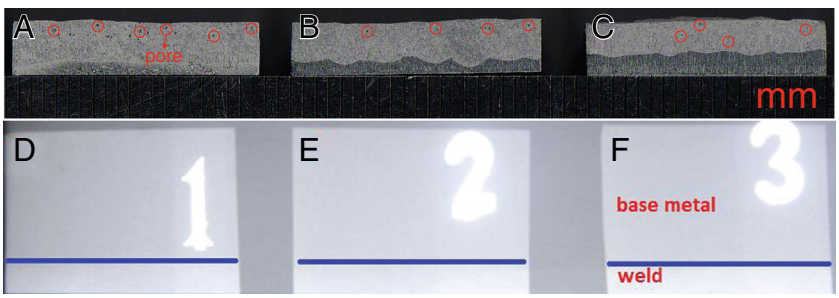

Fig. 9 Longitudinal section of welds (**a** P-GMAW. **b** DP-GMAW. **c** SP-GMAW) and their radiographic images (**d** P-GMAW. **e** DP-GMAW. **f** SP-GMAW)

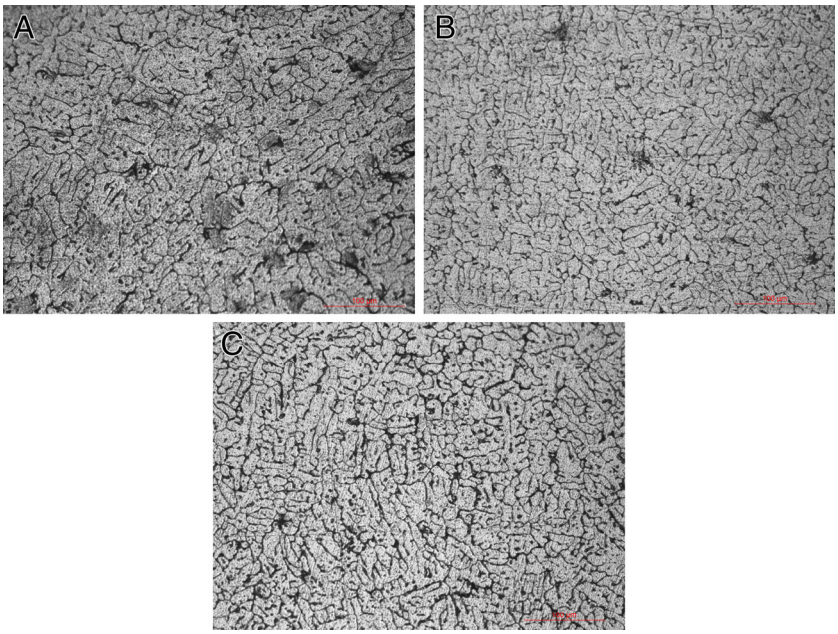

Fig. 10 Microstructure of the fusion zone: **a** P-GMAW. **b** DP-GMAW. **c** SP-GMAW

density distribution. The industrial computer chosen was an Advantech G610, and the data acquisition card chosen was an Advantech PCL-1800. The experimental setup is displayed in Fig. 3.

4.3 Welding parameters and process

Prior to welding, the oxide film on the base metal specimens was ground using abrasive paper (800 grade), followed by degreasing in an acetone solution. The welding seams were obtained from bead-on-plate welds using the P-GMAW, DP-GMAW and SP-GMAW methods with identical parameters, as particularized in Table 2.

Figure 4 presents the transient welding current waveforms and their details after filtering by the self-developed arc dynamic wavelet analyzer. Figure 4c indicates a typical sinusoid modulated current waveform.

4.4 Metallographic and mechanical property processes

After welding, metallographic specimens were obtained by cutting the welded joint, which are perpendicular and parallel to the welding direction using a linear cutting machine, followed by grinding and polishing. The specimens were corroded in Keller agents for 75 s. After washing and drying, the samples were viewed and imaged under cross-polarized light

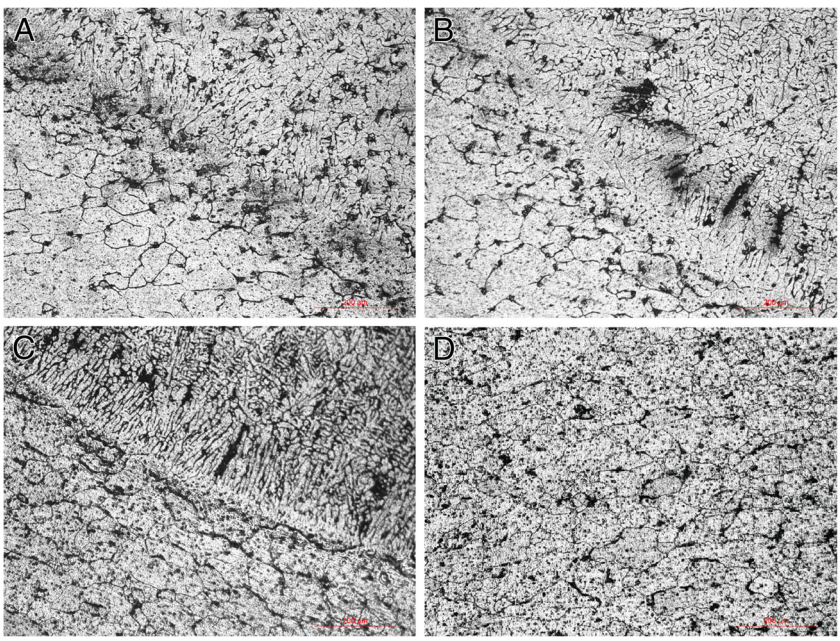

Fig. 11 Microstructure of the HAZ (**a** P-GMAW. **b** DP-GMAW. **c** SP-GMAW) and base metal (**d** AA6061 aluminum alloy)

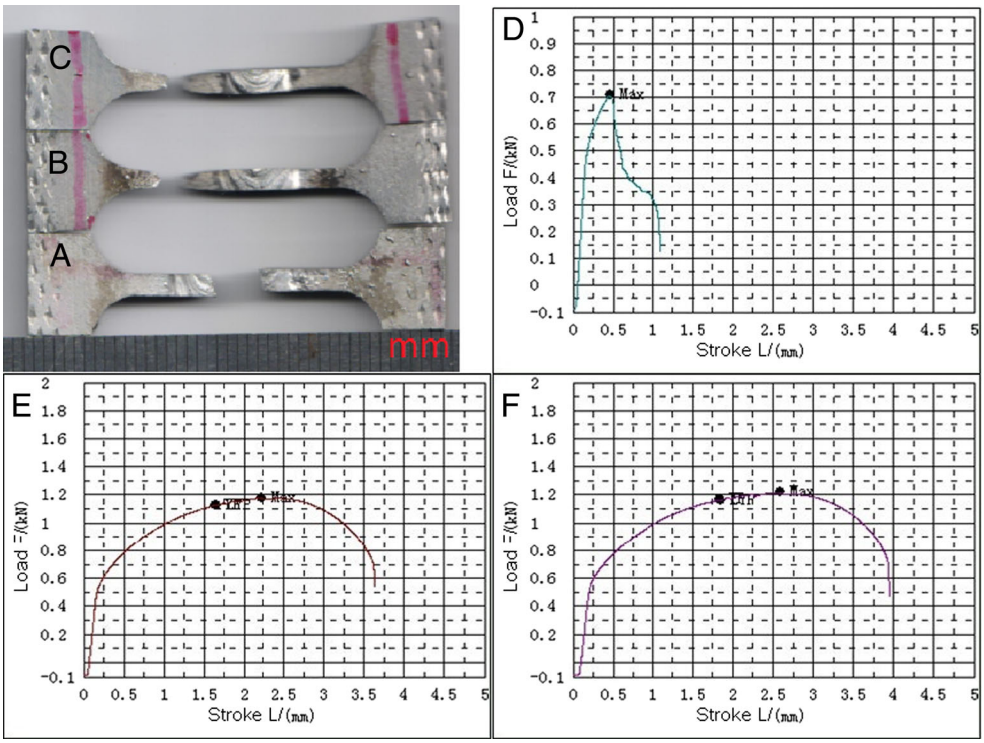

Fig. 12 Fracture location of the joints (**a** P-GMAW. **b** DP-GMAW. **c** SP-GMAW) and tensile curve of the joints (**d** P-GMAW. **e** DP-GMAW. **f** SP-GMAW)

using an optical microscope (LEICA DMI5000M) equipped with a digital camera.

Specimens were ground by abrasive paper (2000 grade) to clean up the corrosive layer. The hardness values were measured using a Vickers microhardness testing machine. Fracture morphologies were imaged using an electron probe microanalyzer (EPMA 1600).

5 Results and discussion

5.1 Welding process stability

Figure 5 exhibits the transient energy waveforms of three different methods. It could be concluded that the energy input in the SP-GMAW process was reduplicated in every period as same as that in the P-GMAW and DP-GMAW processes. Figure 6 demonstrates the dynamic resistance waveforms, and from this figure, it could be concluded that the dynamic resistance was repeated in every period as same as that in the P-GMAW and DP-GMAW processes.

The transient energy and dynamic resistance reflected the welding process stability and should be maintained stable and repeatable in the welding process. No significant differences were observed among the three methods, thereby confirming that the SP-GMAW welding process was as stable as the P-GMAW and DP-GMAW processes. The stability of using the SP-GMAW method to weld aluminum alloy sheets was then verified.

5.2 Weld profile

The photos of weld appearances are displayed in Fig. 7. By analyzing the weld appearance photos, it was possible to conclude that the welding seam was excellently formed by the three welding methods. There was complete penetration between the filler and base metals. Two flanks of welds had clear taenioid areas, which effectively prevented the oxide

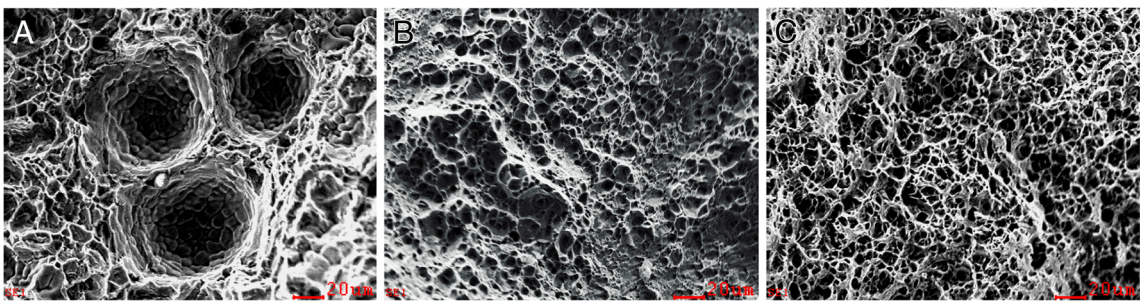

Fig. 13 Fracture morphology of the joints: **a** P-GMAW. **b** DP-GMAW. **c** SP-GMAW

Table 3 Tensile strength and yield strength of the joints

Welding method	Tensile strength (MPa)	Upper yield strength (MPa)	Lower yield strength (MPa)	Fracture location
P-GMAW	114.5	–	–	FZ
DP-GMAW	191.2	182.9	182.7	HAZ
SP-GMAW	197.5	189.2	188.4	HAZ

impurities from mixing into the seam. There was neither burn through nor undercuts in the welds. Lamellar tearing did not occur in the welds. There was very little splashing and overlapping. The bead width was uniform, and the weld surface was clear. There were microgrooves generated by the high-frequency pulse. In addition, there were palpable weld ripples generated by thermal frequency modulation in DP-GMAW and SP-GMAW in contrast with P-GMAW.

The cross section of welds is presented in Fig. 8. Filler metal and the base metal were fully penetrated produced by three welding methods. Each penetration depth of welds exceeded half of the base metal. The difference in weld penetration depth was negligible.

The longitudinal section of welds and their radiographic images are exhibited in Fig. 9. Porosity existed in the weld produced by the P-GMAW appeared more intensive and huger than that produced by the DP-GMAW and SP-GMAW. Figure 13a directly illustrates huge porosities existed in the weld produced by the P-GMAW as well. The DP-GMAW minimized porosity rate distinctly; this result was in agreement with previous research results [26]. The DP-GMAW and SP-GMAW had an identical mechanism in reducing porosity due to thermal pulsation, which would result in fierce weld pool convection and porosity overflowing in contrast with the P-GMAW.

No crack appeared in welds as demonstrated in Fig. 9d, e, and f, respectively. This hazardous weld defect was avoided in the SP-GWAW.

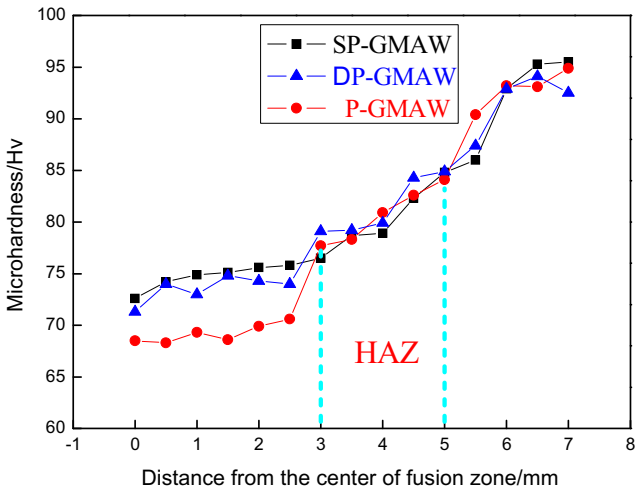

Fig. 14 Microhardness distribution of the joints

These results above revealed that the parameters and energy input were appropriate and that the SP-GMAW was capable of joining aluminum sheet as same as the DP-GMAW.

5.3 Weld microstructure

The microstructure of fusion zone is displayed in Fig. 10. The welds primarily consisted of an α (Al)+Si eutectic structure, and the structural state of the welding joint was dendrite and equiaxed grain.

Grain dimension produced by three welding methods is 24.9, 19.9, and 19.3 μm, respectively. The SP-GMAW method produced more grain refinement of welds of aluminum than did the P-GMAW method. The grain dimension in the SP-GMAW method was homogeneous, and the average grain dimension was small relative to that in the P-GMAW method. There were two reasons for this phenomenon. First, the energy input in the thermal base phase sharply decreased, thereby causing the liquid metal to undercool and further causing surface nucleation that resulted in grain refinement. Second, because the thermal peak phase and thermal base phase periodically alternate, the weld pool surface will rise and fall as the arc force regularly changes, thus enhancing the stir effect on the weld pool. This phenomenon produced intense weld pool convection [27]. The weld pool convection process will cause the molten metal to move forward and back in the weld pool with a certain frequency. The growing grain was broken by scouring and shearing. The grain growth was hindered, and the broken grain would become the nucleation site for a new grain. The SP-GMAW method produced more grain refinement of aluminum welds relative to the DP-GMAW method because the impulse in the SP-GMAW process continuously changed and because the stir effect and convection process on the weld pool were considerably stronger than DP-GMAW. For this reason, the SP-GMAW method produced the finest grains among the three methods.

Microstructure in a heat-affected zone (HAZ) for three welding methods and base metal is presented in Fig. 11. Literature [26] and Fig. 11d revealed that the base metal was mainly consisted of α (Al) and strengthening phase Mg_2Si. Mechanical property loss in the HAZ brought about inferior joint quality, even resulted in joint failure or fracture; focal attention is needed. No melting and solidification happened during welding in the HAZ, but significant solid-phase transformation took place due to a thermal cycle. Results indicated

that coarse grains emerged obviously in the HAZ produced by three welding methods. Grain volume in the HAZ even exceeded that in the base metal, thus proving that recrystallization occurred in a thermal cycle. However, no significant difference in the grain volume of the HAZ was observed among three welding methods because that heat input and linear energy were accurately controlled to be equal by three welding methods.

The SP-GMAW method could produce the finest grain in the fusion zone.

5.4 Tensile property test

Fracture locations and the tensile curves of the joints after tensile tests for three welding methods are exhibited in Fig. 12. For the DP-GMAW and SP-GMAW, fracture is located in the HAZ as shown in Fig. 12b and c. However, fracture occurred in the fusion zone produced by the P-GMAW. Necking deformation stage came out without undergoing yielding stage for joint welded by the P-GMAW, and then fracture occurred. The tensile strength of the fusion zone was less than that of the HAZ and base metal, so the weak link of the joint produced by the P-GMAW is the fusion zone. Porosity dimension in the fusion zone exceeded 90 μm as shown in Fig. 13a. These porosities caused local stress concentration in the fusion zone, then microcrack and microvoid emerged and accumulated in elastic deformation stage. Fracture occurred in the fusion zone when microcrack and microvoid accumulated to a certain extent.

Tensile strength and yield strength of the weld joint are particularized in Table 3. The tensile strength of the DP-GMAW and SP-GMAW far exceeded that of P-GMAW. Both tensile strength and yield strength produced by the SP-GMAW were higher than that produced by the DP-GMAW, but the difference was not obvious.

The fracture morphologies of the joint are demonstrated in Fig. 13. Microstructure in fracture had typical dimple structures, so failure mode for three tensile tests was ductile fracture. There was no significant difference in dimple dimension welded by the DP-GMAW and SP-GMAW as shown in Fig. 13b and c; this result was accordant with tensile curves.

5.5 Weld hardness

Figure 14 displays the Vickers microhardness values of the joints welded by different methods, with all the values measured from the cross section perpendicular to the weld bead.

In the fusion zone, the Vickers microhardness value for SP-GMAW was slightly higher than that for DP-GMAW. The Vickers microhardness for SP-GMAW was obviously higher than that for P-GMAW. From P-GMAW to SP-GMAW, the stirring frequency became close to the resonance frequency of base metal, thereby causing the stirring effect to be more forceful. As a result, the porosity rate in the weld was reduced, and the grain size of the weld was refined, thereby improving the mechanical property of the weld joint.

In the HAZ, difference concerning microhardness of the HAZ and base metal was too negligible to observe.

6 Conclusion

The SP-GMAW welding process was investigated and simplified, and the parameters of the welding procedure were optimized. The feasibility and superiority of the method for welding aluminum sheet were verified. The experimental results indicated that the SP-GMAW method, as an improved DP-GMAW method, has the following features:

1. For three welding methods, welding seams are well formed, no crack existed in the weld joint, and failure mode was ductile fracture. No significant difference was observed concerning welding process stability, HAZ grain dimension, and HAZ microhardness welded by three welding methods.
2. The SP-GMAW minimized porosity rate and generated palpable weld ripples in contrast with the P-GMAW.
3. The SP-GMAW produced the finest fusion zone grain, highest fusion zone microhardness, and highest tensile strength among three welding methods, but the superiority was not obvious compared to the DP-GMAW.

Compliance with ethical standards

Conflict of interest The authors declare that they have no competing interests.

References

1. Park HJ, Kim DC, Kang MJ, Rhee S (2013) The arc phenomenon by the characteristic of EN ratio in AC pulse GMAW. Int J Adv Manuf Technol 66(5-8):867–875. doi:10.1007/s00170-012-4371-1
2. Kranz J, Herzog D, Emmelmann C (2015) Design guidelines for laser additive manufacturing of lightweight structures in TiAl6V4. J Laser Appl 27(S1):S14001. doi:10.2351/1.4885235
3. Stathers PA, Hellier AK, Harrison RP, Ripley MI, Norrish J (2014) Hardness-tensile property relationships for HAZ in 6061-T651 aluminum. Weld J 93(8):301–311
4. Guo WB, Leng XS, Yan JC, Tan YM (2015) Ultrasonic soldering aluminum at low temperature. Weld J 94(6):189S–195S
5. Zhang CY, Chen DL, Luo AA (2014) Joining 5754 automotive aluminum alloy 2-mm-thick sheets using ultrasonic spot welding. Weld J 93(4):131S–138S
6. Han SL, Zeng QL, Lin C, Gao Y, Jia YF (2014) Variation analysis of auto-body aluminum alloy sheet metal assembly in self-pierce riveting. Int J Adv Manuf Technol 70(1-4):701–709. doi:10.1007/s00170-013-5295-0

7. Sortino M, Motyl B, Totis G (2014) Preventive evaluation of mould production cost in aluminium casting. Int J Adv Manuf Technol 70 (1-4):285–295. doi:10.1007/s00170-013-5273-6
8. Tasalloti H, Kah P, Martikainen J (2015) Laser overlap welding of Zn-coated steel on aluminium alloy for patchwork blank applications in the automotive industry. Rev Adv Mater Sci 40(3):295–302
9. Volpone LM, Mueller S (2008) Joints in light alloys today: the boundaries of possibility. Weld Int 22(9):597–609. doi:10.1080/09507110802411518
10. Sánchez-Amaya JM, Delgado T, González-Rovira L, Botana FJ (2009) Laser welding of aluminium alloys 5083 and 6082 under conduction regime. Appl Surf Sci 255(23):9512–9521. doi:10.1016/j.apsusc.2009.07.081
11. Haelsig A, Kusch M, Mayer P (2012) New findings on the efficiency of gas shielded arc welding. Weld World 56(11-12):98–104. doi:10.1007/BF03321400
12. Olabode M, Kah P, Martikainen J (2013) Aluminium alloys welding processes: challenges, joint types and process selection. Proc Inst Mech Eng B J Eng Manuf 227(8):1129–1137. doi:10.1177/0954405413484015
13. Park HJ, Rhee S, Kang MJ, Kim DC (2009) Joining of steel to aluminum alloy by AC pulse MIG welding. Mater Trans 50(9): 2314–2317. doi:10.2320/matertrans.M2009105
14. Kumar S, Dilthey U, Dwivedi DK, Sharma SP, Ghosh PK (2009) Welding of thin sheet of Al alloy (6082) by using vario wire DC P-GMAW. Int J Adv Manuf Technol 42(1-2):102–117. doi:10.1007/s00170-008-1568-4
15. Praveen P, Kang MJ, Yarlagadda PKDV (2008) Drop transfer mode prediction in pulse GMAW of aluminum using statistical model. J Mater Process Technol 201(1-3):502–506. doi:10.1016/j.jmatprotec.2007.11.226
16. Ghosh PK, Dorn L, Hübner M, Goyal VK (2007) Arc characteristics and behaviour of metal transfer in pulsed current GMA welding of aluminium alloy. J Mater Process Technol 194(1-3):163–175. doi:10.1016/j.jmatprotec.2007.04.113
17. Kah P, Suoranta R, Martikainen J (2013) Advanced gas metal arc welding processes. Int J Adv Manuf Technol 67(1-4):655–674. doi:10.1007/s00170-012-4513-5
18. Subramaniam S, White DR, Jones JE (1998) Droplet transfer in pulsed gas metal arc welding of aluminum. Weld J 77(11): 158–464
19. Liu AH, Tang XH, Lu FG (2013) Arc profile characteristics of Al alloy in double-pulsed GMAW. Int J Adv Manuf Technol 68(9-12): 2015–2023. doi:10.1007/s00170-013-4808-1
20. da Silva CLM, Scotti A (2006) The influence of double pulse on porosity formation in aluminum GMAW. J Mater Process Technol 171(3):366–372. doi:10.1016/j.jmatprotec.2005.07.008
21. Vilarinho LO, Scotti A (2000) An alternate algorithm for synergic pulsed GMAW of aluminum. Aust Weld J 45:36–44
22. Wang LL, Jin L, Huang WJ, Xu M, Xue JX (2015) Effect of thermal frequency on AA6061 aluminum alloy double pulsed gas metal arc welding. Mater Manuf Process. doi:10.1080/10426914.2015.1103863
23. Liu AH, Tang XH, Lu FG (2013) Study on welding process and prosperities of AA5754 Al-alloy welded by double pulsed gas metal arc welding. Mater Design 50(9):149–155. doi:10.1016/j.matdes.2013.02.087
24. Wei ZH, Chen XF, Xue JX (2011) Research on sinusoid modulated pulse MIG welding methodology. China Weld 20(4):75–80
25. Wei ZH (2012) Research on current waveform regulation of sinusoid modulated pulse MIG welding in aluminum alloy and expert system. Dissertation, South China University of Technology
26. Mathivanan A, Devakumaran K, Kumar AS (2014) Comparative study on mechanical and metallurgical properties of AA6061 aluminum alloy sheet weld by pulsed current and dual pulse gas metal arc welding processes. Mater Manuf Process 29(8):941–947. doi:10.1080/10426914.2014.912314
27. Becker DW, Jr CMA (2012) The role of pulsed GTA welding variables in solidification and grain refinement. Weld J 58(5):143–152